UNIVERSITY OF
Southampton
Institute of Sound and
Vibration Research

ISVR Technical Report

Theoretical background for a potential real time quantification of gas bubbles in pipelines

T.G. Leighton, K.Baik and J.Jiang

ISVR Technical Report No 335

July 2014

SCIENTIFIC PUBLICATIONS BY THE ISVR

Technical Reports are published to promote timely dissemination of research results by ISVR personnel. This medium permits more detailed presentation than is usually acceptable for scientific journals. Responsibility for both the content and any opinions expressed rests entirely with the author(s).

Technical Memoranda are produced to enable the early or preliminary release of information by ISVR personnel where such release is deemed to the appropriate. Information contained in these memoranda may be incomplete, or form part of a continuing programme; this should be borne in mind when using or quoting from these documents.

Contract Reports are produced to record the results of scientific work carried out for sponsors, under contract. The ISVR treats these reports as confidential to sponsors and does not make them available for general circulation. Individual sponsors may, however, authorize subsequent release of the material.

Theoretical background for a potential real time quantification of gas bubbles in pipelines

T. G. Leighton, K. Baik and J. Jiang

ISVR Technical Report No. 335

June 2014

UNIVERSITY OF SOUTHAMPTON

INSTITUTE OF SOUND AND VIBRATION RESEARCH

FLUID DYNAMICS AND ACOUSTICS GROUP

ACKNOWLEDGEMENTS

This work is supported by the Oak Ridge National Laboratory (ORNL), Tennessee, US. ORNL is managed by UT-Battelle, LLC, under contract DE-AC05-00OR22725 for the US Department of Energy. This work is also funded by the UK Science and Technology Research Council (Principle Investigator: T. G. Leighton). This formulation was developed to assist in understanding acoustic propagation in mercury-filled steel pipes at ORNL, in relate to neutron generation through Spallation Neutron Sources. The authors thank Bernie Riemer and Mark Wendel of ORNL for access to the facilities and helpful discussion of the problem and to Chris Densham, Ottone Caretta, and Tristan Davenne at the UK Science and Technology Research Council for advice and discussions.

CONTENTS

FIGURE CAPTIONS

ABSTRACT

There is a need to measure the quantity of gas bubbles flowing in liquid-filled pipelines in many power, processing and manufacturing industries. This paper outlines the theoretical foundation for one aspect of a candidate bubble detector technique that was commissioned for Oak Ridge National Laboratory's Spallation Neutron Source Target Test Facility (ORNL SPS TTF).

1 Introduction

The authors were commissioned to build ultrasonic technology to quantify the population of helium bubbles in flowing liquid mercury coolant contained with the steel pipelines of the Target Test Facility (TTF) of the Spallation Neutron Source (SNS) at Oak Ridge National Laboratory (ORNL), Tennessee, in. The $1.4 billion SNS is the most powerful pulsed spallation neutron source in the world (figure 1).

Figure 1. Schematic of the Spallation Neutron Source at Oak Ridge National Laboratory, Tennessee. The hydrogen ions for the linear accelerator are generated in the 'front end' building at the top left of the picture, and are accelerated down the linear accelerator (shown in red) to the ring, where protons are accumulated. During repeated circulation of the ring, more protons are added to 'paint out' the complete 200 mm x 70 mm elliptic proton beam. When this is complete (which occurs 60 times per second), the proton pulse is released into the 'target' building, the centre of which houses the sarcophagus in which the actual mercury target is housed. A possible future target building is shown in ghost outline (image courtesy of ORNL).

These detectors would be used on SNS TTF to test the efficacy of candidate bubble injection systems that were being considered for use in SNS. Bubble injection was being considered as a method of reducing erosion in the structure containing the mercury.

SNS produces neutrons that are used by a range of facilities positioned at various angles with respect to the incoming proton beam [1].A limiting factor in the capabilities of the client instruments is the neutron flux that can be transmitted to the samples that they are examining (aircraft wings, forensic material etc.): the greater ('brighter') the flux, the better the instrument performance. In a spallation source, higher flux can be achieved by increasing the power of the proton beam on the target [2].

Although scheduled replacement of the target (the vessel containing the mercury where the proton beam impact occurs) was anticipated in order to take into account radiation embrittlement, late in the facility construction it was recognized that, before radiation damage made target replacement necessary, beam-pulse induced cavitation damage could do so, an effect which would likely increase with increasing beam power. Crucially for the running of such a high value facility, this would mean more frequent target replacements than were envisaged in the operating plans for SNS. Since commissioning in April 2006 (figure 2), SNS beam power was gradually incremented, reaching 1 MW operation with the 2nd operating target. Both targets 1 and 2 were replaced during planned maintenance periods without interruption to the user program. However, in April 2011 unanimous indications from leak detectors in target 3 occurred in the midst of neutron operations.

The cavitation damage of the steel vessel is due to intense pressure pulses in the mercury caused by the micro-second beam pulses [3-6]. Whilst the exact nature of the correlation has not been settled, there is consensus that increasing beam power will in the intended range is likely to significantly increase the erosion [7, 8]. The first target was removed in July 2009 and McClintock *et al.* [9] reported observing significant damage in the interior vessel wall layer that separates the main mercury flow volume from a channel flow that is dedicated to cooling the vessel. In order to realise the beam powers and intervals between target changes that were in the original plan for SNS, an R&D program was initiated to improve understanding of the phenomenon and develop effective damage mitigation technologies for the mercury target [10]. Perhaps the leading candidate solution under development at SNS is to introduce non-condensable helium gas bubbles, either to form a gas wall to protect the steel where the beam enters the target [11, 12], or to provide a population of small bubbles in the bulk of the mercury to absorb the pressure pulse [13] and reduce vapour cavitation formation (and the erosion it generates) on the wall.

The authors were initially funded to develop a broadband device that would provide the bubble size distribution. To develop this they first had to characterise sound propagation in the bubble-free pipe [14, 15] and validate the predictions against a rig of similar pipe dimensions to SNS TTF, but comprising water-filled PMMA pipes (figure 2) as opposed to mercury-filled steel pipes. This demonstrated that the water-filled pipes showed many of the coupling characteristics that complicated the mercury-filled filled at SNS TTF, and so allowed development and deployment of the technique to estimate the bubble size distribution in water-filled PMMA pipes [16].

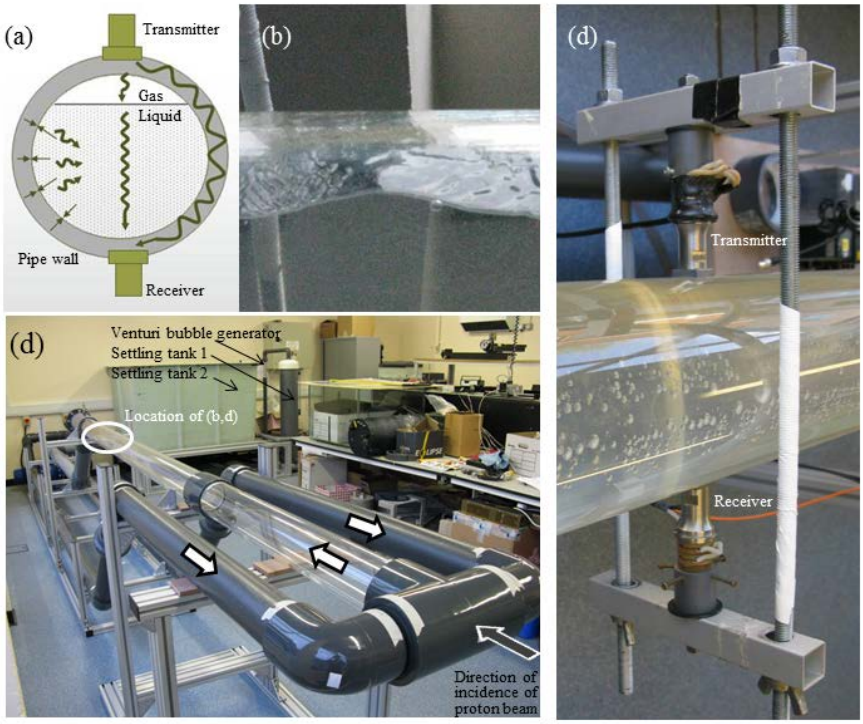

Figure 2. (color online) The 1:1 scale experiment (using water in PMMA tubing) of the relevant part of the mercury-in-steel pipework of SNS TTF. (a) Schematic showing the volume of bubbly liquid used in measuring the dynamic void fraction, and the volume (including the gas pocket at the top of the pipe) used by many other methods of measuring 'void fraction' (such as from calculations based on the mass of gas injected). Curly arrows show three possible routes for propagation between the transmitter and receiver, both of which are clamped onto the outside of the pipe to allow easy relocation and avoid expensive and potentially hazardous ports into the pipe. (b) A photograph of the gas space which occurred in the region shown by the white ellipse in (c), a full-length photo of the pipe rig in which the liquid flow direction is indicated by white arrows with black borders, and the direction of the incoming proton beam (were this SNS) is shown by the grey arrow with a white border. (d) Photograph of one of the designs for source and receiver, mounted on a pipe containing flowing bubbly water (the largest bubbles only are visible): one of the couplers which match the flat transducer faceplate to the curvature of the pipe is visible.

Use of the rig also demonstrated how bubbles in such pipes can collect in large gas pockets trapped at, say, bends in the pipework (figure 2(a,b)), where they do not mitigate erosion (unless, as with the gas wall mentioned above, they are specifically designed to be trapped). Hence it is important to distinguish between the 'dynamic void fraction' (the proportion of the volume of bubbly liquid which is contained in small bubbles that can remain in the flow) and any measure of void fraction which includes the gas trapped in pockets which does not contribute to absorption. Estimates of the void fraction based on monitoring of the mass of gas injected will include the gas spaces trapped within the pipe network. They are therefore not a reliable measure of the 'dynamic void fraction' which reflects the ability of the bubbles to absorb the pressure pulse caused by the impact of the proton beam.

However just as the broadband method was finalised and validated for water-filled pipes [16], plans to construct a device using that method to fit to SNS TTF were curtailed mid-way through this 2-year study by new funding pressures on SNS and STFC R&D. These made the planned 1-1000 kHz frequency range unaffordable. A solution based on clamping narrowband transducers to the outside of the SNS TTF pipes meant the sensor could be readily relocated to track down sources and traps of bubbles, and obviated the need to drill sensor ports in the pipeline (reducing hazard and expense) [17,18]. Whilst this reduced the budget by 80% as required, loss of the information over a wide frequency range would necessarily introduce ambiguities into the interpretation of the acoustical signal, and so ways of interpreting that were sought. The principle was to use the acoustic source to excite circumferential waves in the pipe wall, and these would couple differently to the liquid depending on whether the liquid contained gas bubbles or not [17]. Interpretation of that difference in terms of the bubble population was key, and a suitable way of calculating the wavenumber in bubbly liquid, k'_1 [18]. The first attempt to do this [19] was using the formulation described by Commander and Prosperetti [20]. This method was shown to work provided that the user can make *a priori* a sufficiently accurate estimation of the shape (but not absolute magnitude) of the bubble size distribution [19]. Whilst providing a step forward, it is noted that some industries would not have ready access to this *a priori* information (in SNS TTF, for example, opaque pipes containing an opaque toxic liquid make optical estimate difficult). Other industries that might have difficulty in providing an a priori assessment of the shape of the bubble size distribution are in the manufacture and processing of foodstuffs [21], cement [22], petrochemicals [23], pharmaceuticals [24], and aerosols [25]. Similar issues could occur in the refining and deposition of metals [26], and the management of coolant [27].

2 Experimental scenario

Figure 3 shows the vertical PMMA tube apparatus which allows the acoustic method of monitoring the dynamic void fraction to be compared with a non-acoustic ground-truthing (provided by capturing bubbles in a measuring cylinder via an upturned funnel). This apparatus is similar to that used by Yim and Leighton [17], although the signal processing and associated electronics have been modified (figure 3). In this experiment, the tube is 2 m in length, 4.445 cm in the inner radius and 5 cm in the outer radius. The tube is sealed on one end and is filled with water. Air bubbles are generated via a needle mounted ~20 cm from the bottom, and the total void fraction of bubbles is altered by varying the air flow to the needle form an aquarium air pump (Rena Air-200). The BSD could be measured by the optical method described (with results) in Ref. 16, and gave a range of bubble sizes typically from 30 μm to 1 mm distributed in this pipe system. This realistically matches the difficulties of the ORNL problem, whereby for monochromatic insonification, some bubbles will be driven at, some above, and some below resonance. In this experiment, the Chi-beam sensor pair is driven at a frequency of 41 kHz (the resonance of the high-Q transducers that were adventitiously available at low cost). To be detected appropriately by the Chi-beam sensor, the bubbles should reside sufficiently long within the region of the pipe where the cross-section modes induced by the sensors are formed. In our system this region is typically characterized by the size of coupling cap (here, 5.5 cm diameter). Even a bubble as large as 1 mm radius, which is rare in our system, will take 180~360 ms to cross this region [28]. Almost all the bubbles in this study are smaller, and will stay within the detection range longer than ~200 ms that is the energy storage time of our narrow sensor [as estimated from the Q-factor of the sensor (8500 as measured *in situ*) and the driving frequency of our sensor (41 kHz)]. This means that the energy change due to the pulsation of the bubbles is effectively detected by our narrow band sensor system.

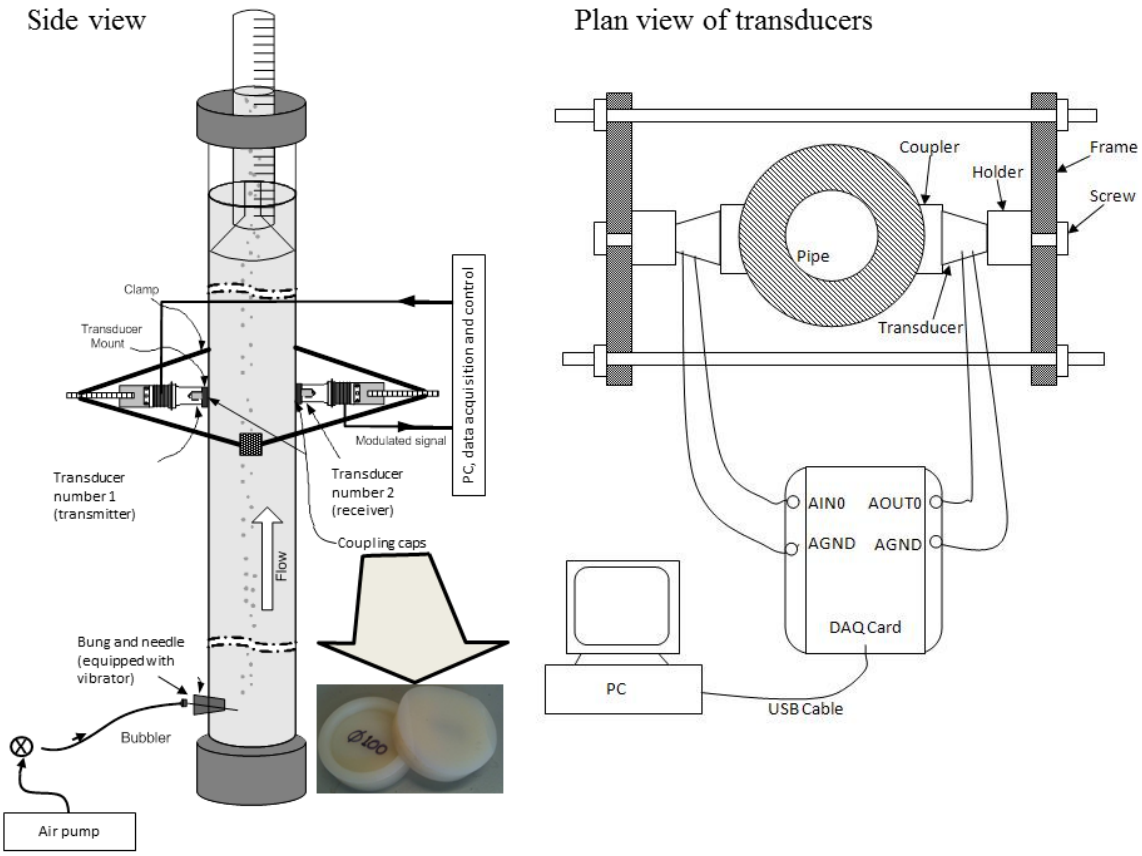

Figure 3. Side view of the vertical pipe test apparatus (with plan view at the level of the transducers) used for validation of the sensor (not to scale). The coupling devices which match the shape (and to a lesser extent, the impedance) of the transducers to the pipe wall, are detailed in the photographic insert. The cap on the left reveals the flat boundary to the transducer and the cap on the right shows the curved boundary that matches the pipe wall.

3 Theory

The objective is to estimate the dynamic void fraction from the EIV derived from the Chi-beam sensor. To investigate the relationship between the signal sent by the source and the one received by the receiver, the circumferential modes (when $k_z \to 0$, where k_z is the axial wavenumber along the z-direction) of the liquid-filled tube are examined using a partial wave series. It is assumed that the source excites the tube, and the receiver records the response, with only cross-sectional motion across the faceplate of each transducer. The route to adapt the theory for phase changes across the transducer is clear but its execution would be laborious, and in this case unnecessary. By considering the pipe wall as a structure coupling to the sensor pair as well as the liquid inside, the output of the

sensor (as detected at the receiver location) responds to the acoustical boundary condition at the sensor position and loading on the inner wall. When only cross-sectional excitation is considered, the pressure at the source location, P_1, can be expressed by the Fourier expansion as:

$$P_1 = \sum_{n=0}^{\infty} p_{1n} \cos n\theta e^{-i\omega t}, \quad p_{1n} = \frac{\varepsilon_n}{\pi} \int_0^{\pi} P_1(\theta') \cos n\theta' d\theta', \tag{1}$$

where θ is the azimuthal angle relative to the source axis (figure 4), and where ε_n equals 1 at n=0 and 2 otherwise (where n is a non-negative integer). For a point source example, $P_1(\theta') = P_{10}\delta(\theta)$ and $p_{1n} = P_{10}\varepsilon_n$. The force caused by the transducer, F, is the product of the radiation impedance, Z_r, and the particle speed of the adjacent media, υ, as follows [29]:

$$F = Z_r \upsilon. \tag{2}$$

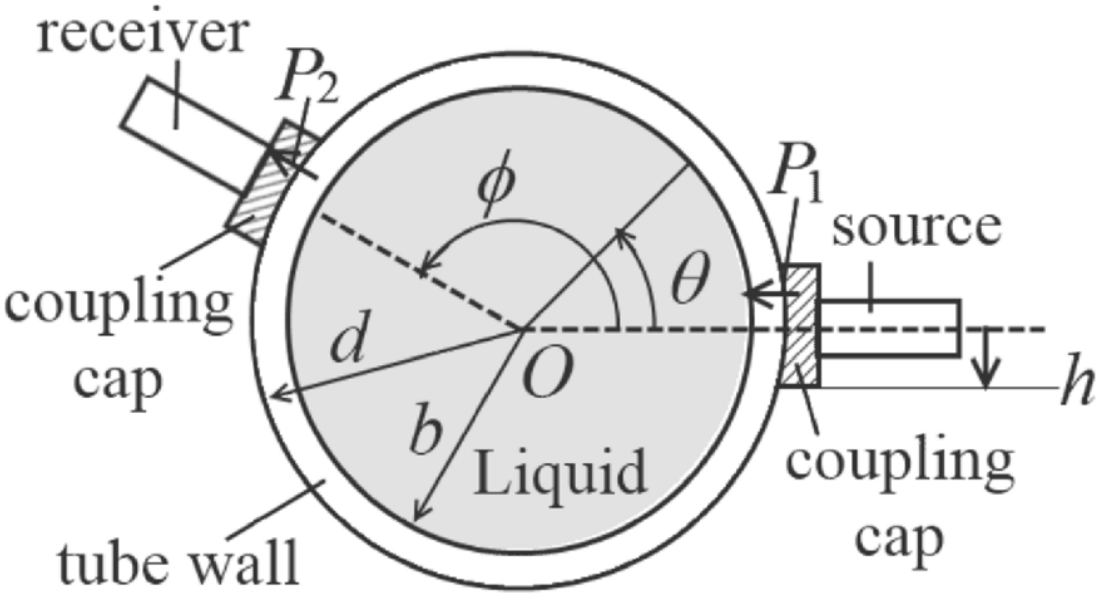

Figure 4. A cross-section of the source, receiver, and the tube filled with liquid inside. The z-axis is perpendicular to the page (out of page). The inner and outer radii of the pipe are b and d, the transducers are mounted in-plane with the pipe cross section and the angle between their beams is ϕ, and θ is the azimuthal angle relative to the source axis. The radius of each coupling cap is h. A pressure, P_2, is measured by the receiver in response to a pressure P_1 applied by the source.

Consequently, the pressure at the receiver, P_2, can be expressed as

$$P_2 = i\omega z_{2a} u_r^e(\theta = \phi), \qquad (3)$$

where z_{2a} is the specific acoustic impedance of the receiver and $u_r^e(\theta = \phi)$ is the radial component of the displacement vector of the elastic solid (tube) at $r=d$ caused by the excitation of P_1. Equation (3) shows that, for a given acoustic excitation, the measured pressure is dependent on the acoustic impedance of the receiver and the magnitude of the normal displacement of the pipe at the location where the receiver is mounted. Once the driving frequency is fixed so that the acoustic impedance of the receiver is fixed, the measured pressure is purely dependent on the magnitude of the normal displacement which is determined by the following matrix equation [18]:

$$u_r^e(\theta) = \frac{1}{2\mu_e}\sum_{n=0}^{\infty}\frac{p_{1n}}{D_n}\times\left[\left(-k_c J_{n+1}^{cd} + \frac{n}{d}J_n^{cd}\right)D_n^{(1)} + \left(-k_c Y_{n+1}^{cd} + \frac{n}{d}Y_n^{cd}\right)D_n^{(2)} + \left(\frac{n}{d}J_n^{sd}\right)D_n^{(3)} + \left(\frac{n}{d}Y_n^{sd}\right)D_n^{(4)}\right]\cos n\theta, \qquad (4)$$

where μ_e is shear modulus of the pipe wall, and k_c and k_s are the longitudinal and shear wavenumbers in the tube material respectively. The Bessel functions, J_{n+1}^{cd} and Y_n^{sd}, are simplified notations for $J_{n+1}(k_c d)$ and $Y_n(k_s d)$ respectively. The elements of the matrix, D, that originate from the elastic boundary conditions on the tube's inner surface (where there is acoustic coupling between the pipe and the liquid) and its outer surface (involving the pipe only), are shown in Appendix A and its determinant is denoted as D_n. The acoustic properties of the liquid are associated with the elements of the matrix, D. The determinant, $D_n^{(m)}$, is obtained by substituting the m-th column of matrix D with the transposition of the vector, $[0 \quad 0 \quad 0 \quad 1]$. The introduction of bubbles into the liquid changes Q_n in the element of $d_{31}\sim d_{34}$ of matrix D which substitutes wavenumber k_0 in pure liquids with k_m in bubbly liquids.

Although the evaluations of Eqs. (3) and (4) are ideally infinite summations, each actual summation is truncated up to the maximum of the mode index, n, which satisfies $n \le \pi/\left[2\sin^{-1}(h/d)\right]$. Here, h is the half width of the flat side of the coupling cap, which is a machined plastic coupler that is flat at its boundary to the transducer but curved to match the boundary with the pipe (Figs. 2 and 4). This relationship follows from the condition that the size of the aperture should be less than half the

wavelength of the circumferential waves along the outer surface of the tube, which allows the mode to be excited by a piston-like transducer.

4 Conclusions

Having completed the theoretical investigations outlined in section 3, for the experimental scenario discussed in section 2, the issue now is the route by which the wavenumber in bubbly liquid, k_m, is evaluated in the formulation, as this will determine in large part the *a priori* information required to cause the algorithm to converge to an acceptable answer. Reference [19] examines the advantages and disadvantages of using the formulation developed by Commander and Prosperetti [20].

Appendix A: Matrix elements of Eq. (4)

$$d_{11} = \frac{nk_c}{b} J_{n+1}(k_c b) - \frac{n(n-1)}{b^2} J_n(k_c b),$$
$$d_{12} = \frac{nk_c}{b} Y_{n+1}(k_c b) - \frac{n(n-1)}{b^2} Y_n(k_c b),$$
$$d_{13} = -\frac{k_s}{b} J_{n+1}(k_s b) + \left\{ \frac{k_s^2}{2} - \frac{n(n-1)}{b^2} \right\} J_n(k_s b),$$
$$d_{14} = -\frac{k_s}{b} Y_{n+1}(k_s b) + \left\{ \frac{k_s^2}{2} - \frac{n(n-1)}{b^2} \right\} Y_n(k_s b),$$

$$d_{21} = \frac{nk_c}{d} J_{n+1}(k_c d) - \frac{n(n-1)}{d^2} J_n(k_c d),$$
$$d_{22} = \frac{nk_c}{d} Y_{n+1}(k_c d) - \frac{n(n-1)}{d^2} Y_n(k_c d),$$
$$d_{23} = -\frac{k_s}{d} J_{n+1}(k_s d) + \left\{ \frac{k_s^2}{2} - \frac{n(n-1)}{d^2} \right\} J_n(k_s d),$$
$$d_{24} = -\frac{k_s}{d} Y_{n+1}(k_s d) + \left\{ \frac{k_s^2}{2} - \frac{n(n-1)}{d^2} \right\} Y_n(k_s d),$$

$$d_{31} = k_c \frac{1+bQ_n}{b} J_{n+1}(k_c b) + \left\{ P + \frac{n(n-1-bQ_n)}{b^2} \right\} J_n(k_c b),$$

$$d_{32} = k_c \frac{1+bQ_n}{b} Y_{n+1}(k_c b) + \left\{ P + \frac{n(n-1-bQ_n)}{b^2} \right\} Y_n(k_c b),$$

$$d_{33} = -\frac{nk_s}{b} J_{n+1}(k_s b) + \frac{n(n-1-bQ_n)}{b^2} J_n(k_s b),$$

$$d_{34} = -\frac{nk_s}{b} Y_{n+1}(k_s b) + \frac{n(n-1-bQ_n)}{b^2} Y_n(k_s b),$$

$$d_{41} = \frac{k_c}{d} J_{n+1}(k_c d) + \left\{ P + \frac{n(n-1)}{d^2} \right\} J_n(k_c d),$$

$$d_{42} = \frac{k_c}{d} Y_{n+1}(k_c d) + \left\{ P + \frac{n(n-1)}{d^2} \right\} Y_n(k_c d),$$

$$d_{43} = -\frac{nk_s}{d} J_{n+1}(k_s d) + \frac{n(n-1)}{d^2} J_n(k_s d),$$

$$d_{44} = -\frac{nk_s}{d} Y_{n+1}(k_s d) + \frac{n(n-1)}{d^2} Y_n(k_s d),$$

where

$$Q_n = \frac{\rho_0 \omega^2}{2\rho_e c_s^2} \frac{J_n(k_0 b)}{k_0 J_{n+1}(k_0 b) - \frac{n}{b} J_n(k_0 b)}, \quad P = -\frac{k_s^2}{2}.$$

Here ρ_0 and ρ_e are the densities of the liquid and tube respectively, c_s is shear speed in the tube, and k_0 is wavenumber in bubble-free liquid.

References

1. Mason T.E., Abernathy, D., Anderson, I., Ankner, J., Egami, T., Ehlers, G., Ekkebus, A., Granroth, G., Hagen, M., Herwig, K., Hodges, J., Hoffmann, C., Horak, C., Horton, L., Klose, F., Larese, J., Mesecar, A., Myles, D., Neuefeind, J., Ohl, M., Tulk, C., Wang, X.-L. & Zhao, J. 2006 The Spallation Neutron Source in Oak Ridge: A powerful tool for materials research. *Physica B* **385–386**(2), 955–960.

2. Gabriel, T.A., Haines, J.R., McManamy, T.J., Spampinato, P. & Riemer, B.W. 2001 Targets for high-intensity particle production. *Proc. 2001 Particle Accelerator Conference*, 2001 (Chicago, IL, USA, 18 Jun 2001 - 22 Jun 2001) Vol. 1, pp. 737 – 741(doi: 10.1109/PAC.2001.987619)

3. Futakwa, M., Kogawa, H., Hasegawa, S., Ikeda, Y., Riemer, B., Wendel, M., Haines, J., Bauer, G., Naoe, T., Tanaka, N., Okita, K., Fijiwara, A. & Matsumoto, Y. 2006 Cavitation erosion by proton beam bombarding mercury target for spallation neutron source. *Proc. Sixth Int. Symp. on Cavitation*, Wageningen, The Netherlands (2006) 6 pages.

4. Futakawa, M., Kogawa, H., Hasegawa, S., Ikeda, Y., Riemer, B., Wendel, M., Haines, J., Bauer, G., Naoe, T., Okita, K., Fijiwara, A., Matsumoto, Y. & Tanaka, N. 2008 Cavitation damage prediction for spallation target vessels by assessment of acoustic vibration. *J. Nuclear Materials* **77**, 182-188.

5. Riemer, B. 2005 Benchmarking dynamic strain predictions of pulsed mercury spallation target vessels. *J. Nucl. Materials* **343**, 81–91.

6. Manzi, N. J., Chitnis, P. V., Holt, R. G., Roy, R. A., Cleveland, R. O., Riemer, B. & Wendel, M. 2010 Detecting cavitation in mercury exposed to a high-energy pulsed proton beam. *J. Acoust. Soc. Am.***127**, 2231-2239.

7. Haines, J. ,Riemer, B., Felde, D., Hunn, J., Pawel, S. & Tsai, C. 2005 Summary of cavitation erosion investigations for the SNS mercury target. *J. Nuclear Materials* **343**, 58–69.

8. Riemer, B. W., Abdou, A., Felde, D. K., Sangrey, R. L. &Wendel, M. W. 2010 Results from cavitation damage experiments with mercury spallation targets at the LANSCE – WNR in 2008.*Proc. 19th meeting on Collaboration of Advanced Neutron Sources* (ICANS XIX, March 8 – 12, 2010, Grindelwald, Switzerland), 9 pages.

9. McClintock, D.A., Riemer, B.W., Ferguson, P.D., Carroll, A.J. & Dayton, M.J., Initial observations of cavitation-induced erosion of liquid metal spallation target vessels at the Spallation Neutron Source Journal of Nuclear Materials 431 (2012) 147–159

10. Riemer, B. W., Wendel, M. W., Felde, D. K., Abdou, A. & McClintock, D. A., Status of R&D on mitigating the effects of pressure waves for the Spallation Neutron Source mercury target, Journal of Nuclear Materials 431 (2012) 160–171

11. Felde, D., Riemer, B. & Wendel, M. 2008 Development of a gas layer to mitigate cavitation damage in liquid mercury spallation targets. *J. Nuclear Materials* **377**, 155-161.

12. Chitnis, P. V., Manzi, N. J., Cleveland, R. O., Roy, R. A. & Holt, R. G. 2010 Mitigation of damage to solid surfaces from the collapse of cavitation bubble clouds. *J. Fluids Engineering* **132**, 051303-1 - 051303-6.

13. Leighton, T. G., Jiang, J. & Baik, K. 2012 Demonstration comparing sound wave attenuation inside pipes containing bubbly water and water droplet fog. *J. Acoust. Soc. Am.* **131**(3 Pt 2), 2413-2421. (DOI: 10.1121/1.3676732).

14. Baik, K, Jiang, J. & Leighton, T. G. 2010 Acoustic attenuation, phase and group velocities in liquid-filled pipes: theory, experiment, and examples of water and mercury. *J. Acoust. Soc. Am.***128**, 2610-2624.

15. Jiang, J., Baik, K. & and Leighton, T. G. 2011 Acoustic attenuation, phase and group velocities in liquid-filled pipes II: Simulation for spallation neutron sources and planetary exploration. *J. Acoust. Soc. Am.***130**, 695-706.

16. Leighton, T.G., Baik, K. & Jiang, J. 2012 The use of acoustic inversion to estimate the bubble size distribution in pipelines, *Proceedings of the Royal Society A*, 468, 2461-2484.

17. Yim, G. T. & Leighton, T. G. 2010 Real-time on-line monitoring of ceramic "slip" in pottery pipe-lines using ultrasound. *Ultrasonics* **50**, 60-67.

18. Baik, K, Jiang, J. & Leighton, T. G. 2012 Acoustic attenuation, phase and group velocities in liquid-filled pipes III: Non-axisymmetric propagation and circumferential modes in lossless conditions. *J. Acoust. Soc. Am.* **133** (2), 1225–1236 (2012). [doi: 10.1121/1.4773863].

19. Baik, K., Leighton, T. G., & Jiang, J. 2014 Investigation of a possible method for real time quantification of gas bubbles in pipelines, *J. Acoust. Soc. Am.,* (accepted).

20. Commander, K. W. & Prosperetti, A. 1989 Linear pressure waves in bubbly liquids: Comparison between theory and experiments, *J. Acoust. Soc. Am.* **85**, 732-746.

21. Campbell, G. M. & Mougeot, E. 1999 Creation and characterisation of aerated food products, *Trends Food Sci. Technol.* **10**, 283–296.

22. Punurai, W., Jarzynski, J., Qu, J., Kurtis, K. E. & Jacobs, L. J. 2006 Characterization of entrained air voids in cement paste with scattered ultrasound. *NDT & E Int.***39**, 514–524.

23. Leighton, T.G. & White, P.R. 2012 Quantification of undersea gas leaks from carbon capture and storage facilities, from pipelines and from methane seeps, by their acoustic emissions, *Proc. Royal Soc. A,* 468, 485-510.

24. Stride, E. P. & Coussios, C. C. 2010 Cavitation and contrast: The use of bubbles in ultrasound imaging and therapy. *Proceedings of the Institution of Mechanical Engineers, Part H: Journal of Engineering in Medicine*, **224**, 171-191.doi: 10.1243/09544119JEIM622

25. Maksimov, A.O. & Leighton, T.G. 2012 Pattern formation on the surface of a bubble driven by an acoustic field, *Proceedings of the Royal Society A,* 468, 57-75.

26. Offin, D.G., Birkin, P.R. & Leighton, T. G. 2007 Electrodeposition of copper in the presence of an acoustically excited gas bubble, *Electrochemistry Communications,* **9**, 1062-1068.

27. Winterton, R.H.S. 1972 Cover-gas bubbles in recirculating sodium primary coolant, Nuclear Engineering and Design, 22(2), 262–271.

28. Clift, R., Grace, J. R. and Weber, M. E. 1978 Bubbles, Drops, and Particles (Academic Press, New York), pp. 171-173)